# 큰 받음각을 갖는 세장형 물체 주위의 점성 유동장 수치 모사

# Numerical Simulation of Flow Around a Slender Body at High Angle of Attack

노 오현[1] ,          황 수정[2]
Oh Hyun Rho  and  Soo Jung Hwang

## ABSTRACT

The compressible laminar and turbulent viscous flow on a slender body in supersonic speed as well as subsonic speed has been numerically simulated at high angle of attack. The steady and time-accurate compressible thin-layer Navier-Stokes code based on an implicit upwind-biased LU-SGS algorithm has been developed and specifically applied at angles of attack of 20, 30, 40 deg, respectively. The modified eddy-viscosity turbulence model suggested by Degani and Schiff was used to simulate the case of turbulent flow. Any geometric asymmetry and numerical perturbation have not been intentionally or artificially imposed in the process of computation. The purely numerical results for laminar and turbulent cases, however, show clear asymmetric formation of vortices which were observed experimentally. Contrary to the subsonic results, the supersonic case shows the symmetric formation of vortices as indicated by the earlier experiments.

## INTRODUCTION

Recently, as the development of many highly maneuverable aircraft and missiles capable of controlled flight at high angle of attack have been needed, the physical understanding of these flowfields has become a very important subject. Above all, the most important characteristics of high angle of attack flow are that asymmetric vortices arise on the leeward side of the very nearly symmetric slender bodies and these vortices produce sizable side forces and yawing moments, thereby can exert a significant influence on the longitudinal and lateral flight controls.

A large number of experimental[1-4] and computational[5-12] studies had been carried out by many investigators in order to find out the origin of the asymmetric features and the physically corresponding behaviors, but the nature of the asymmetry is extremely difficult to determine either by experiment or computation, since neither are perfect simulations. For example, experiments suffer from the inability to manufacture a perfectly symmetric nose tip and freestream nonuniformities. Computations suffer from truncation, round-off errors and convergence difficulties, etc.

Two approaches, absolute and convective instabilities, have been offered to explain the nature of the observed asymmetries[11]. In essence, if the instability is absolute, any initial asymmetric disturbance grows exponentially at any fixed location. For a large time, the exponential growth will be limited by nonlinearities and thereby asymmetries can be induced by a transient asymmetric disturbance. If, on the other hand, the instability is convective, although the initial disturbance grows with time, it is convected downstream, and after sufficiently large time, the basic flow becomes again symmetric.

Referred to as a convective-type asymmetry, this point of view is supported by the time-accurate compressible Navier-Stokes computations of Degani et al.[5-8] for the laminar and turbulent subsonic flows over a tangent ogive-cylinder at high angle of attack, where steady asymmetries were observed only when a fixed spatial asymmetry was intentionally imposed. Removal of the asymmetry always led to a return to symmetric flow.

On the other hand, supersonic laminar computations by Siclari and Marconi[9] have demonstrated asymmetries of the absolute instability type using the approximate conical Navier-Stokes equations. Also, the incompressible three-dimensional turbulent Navier-Stokes computations of Hartwich et al.[10] for a tangent ogive body at an angle of attack of 40 deg have indicated an asymmetric flowfield without the imposition of a fixed geometric asymmetry in the computation. Vanden and Belk[11] have showed that the unsymmetric factorization error in the transient solution can produce asymmetric flow without the introduction of any geometric and initial asymmetry using thin-layer laminar Navier-Stokes equations with a two-pass implicit approximate factorization.

In this paper, the implicit upwind methods for computing the three-dimensional laminar and turbulent compressible viscous flow based on ADI[14] and LU-SGS[15,16] algorithms have been developed and applied to investigate whether the type of factorization, without imposing any geometric asymmetry, can be an essential cause of the numerical asymmetric perturbation that may produce asymmetric flowfield. The computed results for laminar flow are compared with those of experiments carried out by Lamont[2,3]. In computing a turbulent flow, the turbulence model modified by Degani and Schiff[18] which accounts reasonably well the presence of the leeward side vortex structure is used. The numerical results are compared with the existing experimental data. The computation on laminar supersonic flow is also carried out for phenomenal comparison to subsonic results.

1. 서울대학교 항공우주공학과 (151-742, 서울시 관악구 신림 동 산 56-1, Tel: 02-880-7381)
2. 서울대학교 항공우주공학과 공기역학실(Tel: 02-880-7391)

# THEORETICAL BACKGROUND

## Governing Equations

The governing equations are the thin layer approximations to the three dimensional, time-dependent, compressible Navier-Stokes equations, and are written in generalized coordinates and conservation law form as

$$\partial_\tau \hat{Q} + \partial_\xi \hat{E} + \partial_\eta \hat{F} + \partial_\zeta (\hat{G} - \hat{G}_v) = 0 \tag{1}$$

where $\zeta$ corresponds to the coordinate normal to the body surface. The flux vectors are

$$Q = \frac{1}{J}\begin{bmatrix} \rho \\ \rho u \\ \rho v \\ \rho w \\ \rho e \end{bmatrix} \quad , \quad \hat{E} = \frac{1}{J}\begin{bmatrix} \rho U \\ \rho Uu + \xi_x p \\ \rho Uv + \xi_y p \\ \rho Uw + \xi_z p \\ (\rho e + p)U \end{bmatrix}$$

$$\hat{F} = \frac{1}{J}\begin{bmatrix} \rho V \\ \rho Vu + \eta_x p \\ \rho Vv + \eta_y p \\ \rho Vw + \eta_z p \\ (\rho e + p)V \end{bmatrix} \quad , \quad \hat{G} = \frac{1}{J}\begin{bmatrix} \rho W \\ \rho Wu + \zeta_x p \\ \rho Wv + \zeta_y p \\ \rho Ww + \zeta_z p \\ (\rho e + p)W \end{bmatrix} \tag{2}$$

$$\hat{G}_v = \frac{\mu}{ReJ}\begin{bmatrix} 0 \\ m_1 u_\zeta + m_2 \zeta_x \\ m_1 v_\zeta + m_2 \zeta_y \\ m_1 w_\zeta + m_2 \zeta_z \\ m_1 m_3 + m_2(\zeta_x u + \zeta_y v + \zeta_z w) \end{bmatrix}$$

where
$$\begin{aligned} m_1 &= \mu(\zeta_x^2 + \zeta_y^2 + \zeta_z^2) \\ m_2 &= \mu/3(\zeta_x u_\zeta + \zeta_y v_\zeta + \zeta_z w_\zeta) \\ m_3 &= 1/2(u^2 + v^2 + w^2) + Pr^{-1}(\gamma-1)^{-1}(a^2)_\zeta \end{aligned} \tag{3}$$

and Pr is Prandtl number, Re is Reynolds number based on cylinder diameter, J is the determinant of transformation Jacobian matrix and contravariant velocity components U, V, and W are defined as

$$\begin{aligned} U &= \xi_x u + \xi_y v + \xi_z w \\ V &= \eta_x u + \eta_y v + \eta_z w \\ W &= \zeta_x u + \zeta_y v + \zeta_z w \end{aligned} \tag{4}$$

The equation of state is needed to complete the set of equations, that is

$$p = \rho(\gamma-1)[e - 1/2(u^2 + v^2 + w^2)] \tag{5}$$

where $\gamma$ is the ratio of specific heats.

## Numerical Algorithm

The governing equations are solved with a finite-volume algorithm for both steady and unsteady flow calculations. The convective and pressure terms are upwind differenced using the flux difference splitting scheme of Roe, and the shear stress and heat transfer terms are centrally differenced. The convective and pressure terms are differenced using the monotone upstream-centered schemes for conservation laws (MUSCL) approach, and minmod and differential limiters are used to suppress nonphysical oscillations near discontinuities.

In this study two algorithms, alternating direction implicit (ADI) scheme by Beam and Warming and lower upper symmetric Gauss-Seidel (LU-SGS) implicit scheme by Yoon and Jameson are used, respectively, to ensure numerical symmetry in the crossflow plane. Because of

three factors, the ADI scheme introduces the error terms of $(\Delta t)^3$ and needs the considerable memory and computing time.

$$[\frac{I}{J\Delta t} + D_\xi^- \hat{A}^+ + D_\xi^+ \hat{A}^-][\frac{I}{J\Delta t} + D_\eta^- \hat{B}^+ + D_\eta^+ \hat{B}^-]$$
$$[\frac{I}{J\Delta t} + D_\zeta^- \hat{C}^+ + D_\zeta^+ \hat{C}^-]\Delta\hat{Q} = -\hat{R} \tag{6}$$

But LU-SGS scheme requires no additional relaxation of factorization on planes of sweep, thus can reduce lots of memory and computing time in three dimensional computation. The LU-SGS scheme can be written as

$$(LD^{-1}U)\Delta\hat{Q} = -\hat{R} \tag{7}$$

where
$$\begin{aligned} L &= \frac{I}{J\Delta t} + D_\xi^- \hat{A}^+ + D_\eta^- \hat{B}^+ + D_\zeta^- \hat{C}^+ - \hat{A}^- - \hat{B}^- - \hat{C}^- \\ D &= \frac{I}{J\Delta t} + \hat{A}^+ - \hat{A}^- + \hat{B}^+ - \hat{B}^- + \hat{C}^+ - \hat{C}^- \\ U &= \frac{I}{J\Delta t} + D_\xi^+ \hat{A}^- + D_\eta^+ \hat{B}^- + D_\zeta^+ \hat{C}^- + \hat{A}^+ + \hat{B}^+ + \hat{C}^+ \end{aligned} \tag{8}$$

The Jacobian matrices of the flux vectors are constructed approximately to yield diagonal dominance

$$\hat{A}^\pm = \frac{\hat{A} \pm \rho(\hat{A})I}{2} \quad \text{and} \quad \rho(\hat{A}) = \beta\max[|\lambda(\hat{A})|] \tag{9}$$

where $\lambda(\hat{A})$ represents eigenvalues of Jacobian matrix $\hat{A}$ and $\beta$ is a constant that is greater than or equal to 1.

The above factored equation is solved as a series of following sweeps of the scalar inversion

$$\begin{aligned} L\Delta\hat{Q}^* &= -\hat{R} \\ U\Delta\hat{Q} &= D\Delta\hat{Q}^* \end{aligned} \tag{10}$$

and vectorized on i+j+k=constant oblique planes of sweep.

## Turbulence Models

The coefficients of viscosity and thermal conductivity which appear in eq.(2) are given independently from auxiliary relations. For laminar flows, the coefficient of viscosity is obtained using Sutherland's law, while for turbulent flow the coefficient is obtained from the eddy-viscosity turbulence model modified by Degani and Schiff.[7,8,18] The coefficient of thermal conductivity is obtained once the viscosity coefficient is known by assuming a constant Prandtl number.

Degani and Schiff developed a modification to the well-known Baldwin-Lomax algebraic model[17] for high angle of attack flows. The modifications extend the model in a rational manner to permit an accurate determination of the viscous length scale for high angle of attack flows in regions of crossflow separation, where a strong leeward vortical flow structure exists.

The viscosity $\mu$ and coefficient of thermal conductivity $\kappa$ are assumed to be the sum of the laminar flow coefficients and turbulent flow coefficients, i.e.,

$$\mu = \mu_l + \mu_t \tag{11}$$

$$\frac{\kappa}{c_p} = \frac{\mu_l}{Pr_l} + \frac{\mu_t}{Pr_t} \tag{12}$$

where the turbulent eddy viscosity $\mu_t$ is defined as

$$\mu_t = \min[\ (\mu_t)_{inner}\ ,\ (\mu_t)_{outer}\ ] \qquad (13)$$

In the inner region, the Prandtl-Van Driest formulation is used to determine $\mu_t$. This formula is defined as

$$(\mu_t)_{inner} = \rho l^2 \Omega \qquad (14)$$

where

$$l = ky^+[\ 1.0\ -\ e^{-(y^+/A^+)}] \qquad (15)$$

$$y^+ = \frac{\rho_w u_\tau y}{\mu_w} = \frac{\sqrt{\rho_w \tau_w y}}{\mu_w} \qquad (16)$$

$$\Omega = \sqrt{(u_y - v_x)^2 + (v_z - w_y)^2 + (w_x - u_z)^2} \qquad (17)$$

In the outer region, for attached boundary layers, $\mu_t$ is determined by using of the following equation

$$(\mu_t)_{outer} = \rho K C_{cp} F_{wake} F_{Kleb}(y) \qquad (18)$$

In eq.(18),

$$F_{wake} = \min[\ (y_{max}F_{max})\ ,\ (C_{wk}y_{max}u_{dif}^2)] \qquad (19)$$

where $u_{dif}$ is the difference between the maximum and minimum total velocity in the local profile

$$u_{dif} = (\sqrt{u^2 + v^2 + w^2})_{max} - (\sqrt{u^2 + v^2 + w^2})_{min} \qquad (20)$$

and $F_{Kleb}$ is the Klebanoff intermittency factor

$$F_{Kleb}(y) = \left[\ 1.0\ +\ 5.5\left(\frac{C_{Kleb}y}{y_{max}}\right)^6\right]^{-1} \qquad (21)$$

The quantity $F_{max}$ is defined as the maximum that the following function

$$F(y) = y\Omega[\ 1.0\ -\ e^{-(y^+/A^+)}] \qquad (22)$$

takes in the local profile and $y_{max}$ is the normal distance from the surface at which $F_{max}$ occurs in the original Baldwin-Lomax turbulence model. The constants that appear in the proceeding equations are given in Ref.17. But a problem with the Baldwin-Lomax model is encountered when it is applied to treat flow around slender bodies at high angle of attack. In this flow, the regions of crossflow separation is dominant. In a region where a vortex structure resulting from crossflow separation exists, the function F(y) has two or three relative maxima. If the Baldwin-Lomax model is used to search the entire flowfield normal to a surface point for $F_{max}$, the second or third maximum in F(y) is obtained, rather than the desired peak based on the underlying boundary layer. This results in too much high values of $F_{max}$ and $y_{max}$, resulting in a distortion or a washout of the features in the computed flow. To address this problem, Degani and Schiff[18] proposed a modification to the application of the model. Instead of searching outward along the entire radial ray for the value of $F_{max}$ at each surface grid point, the search for a maximum of F(y) stops after the first peak. The details of Degani-Schiff modification model are given in Ref.7,8,19.

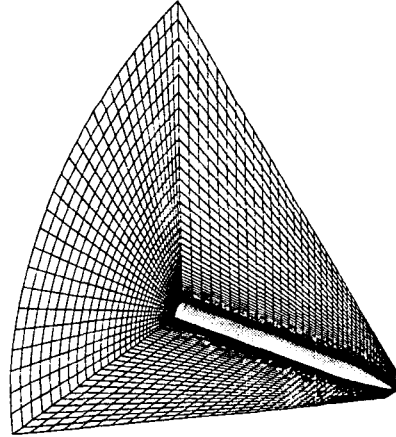### Body configurations and Computational Grids

Computations were performed for subsonic and supersonic flows over an ogive-cylinder body, which consisted of 3.5 diameter tangent ogive forebody with a 8.5 diameter cylindrical afterbody extending aft of the nose-body junction to x/D = 12. This body geometry has been extensively tested by Lamont[2,3].

The grid consisted of 90 circumferential planes extending completely around the body. In each circumferential plane, the grid contained 50, 60 radial points between the body surface and the computational outer boundary and the 45 axial points between the nose and the rear of the body. The grids were exactly symmetric between left and right sides, Fig.1 shows the subsonic and supersonic grid.
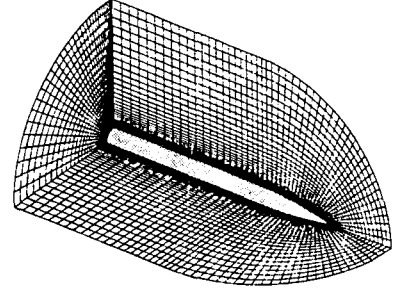


(a) subsonic grid



(b) supersonic grid

Fig. 1 Computational grid around tangent ogive-cylinder

### Boundary Conditions and Initial Conditions

An adiabatic no-slip boundary condition was applied at the body surface, the characteristic boundary conditions and undisturbed freestream conditions are maintained at the computational outer boundary in subsonic and supersonic cases respectively. At the downstream boundary, nonreflecting boundary condition was applied to subsonic flow and the simple extrapolation to supersonic flow.

In these computations, unsteady, time-accurate solutions were calculated together with the steady-state solutions. Thus, the first-order time accurate algorithm was used with a globally constant time step to the unsteady solutions. The flowfield was initially set to freestream conditions throughout the grid or to a previously obtained solution, and the flowfield was advanced in time until a converged solution reached.

## RESULTS and DISCUSSION

A series of flow computation around a tangent ogive-cylinder body in subsonic and supersonic speed has been systematically arranged in order to understand physically the causal process of asymmetric vortex formation which were observed experimentally. The systematic computations are arranged as follows ;

**Case 1 : Algorithmic Study**

It is essentially concerned with exploration of how the different numerical algorithms affect symmetry breakdown and where the origin of asymmetric perturbation or numerical error comes from.

**Case 2 : Subsonic Laminar Flow**

The unsymmetric factorization algorithm has been applied for the flow of $Re_D=2.0\times10^5$ and $M_\infty=0.2$.

**Case 3 : Subsonic Turbulent Flow**

The computation has been carried out by applying the unsymmetric factorization algorithm, using the unmodified and modified turbulence model suggested by Degani and Schiff.

**Case 4 : Supersonic Laminar Flow**

In order to investigate possibility of the formation of vortex on leeward side, the supersonic laminar flow computation has been performed for $M_\infty=2.0$.

A time-accurate (unsteady) and steady-state solutions have been obtained by starting from the freestream initial conditions or from the previous calculations. The solution was considered to have converged to a steady state after error (L2NORM) dropped at least four orders of magnitude from initial starting.

*Effects of Algorithm on Asymmetry*

The histories of computed side-force coefficients for three algorithms which are ADI, steady and unsteady LU-SGS are shown in Fig.2. Computations were all carried out for a Reynolds number based on cylinder diameter, $Re_D$, of $2.0\times10^5$ and $M_\infty=0.2$, $\alpha=40$ deg. Steady and unsteady (time-accurate) LU-SGS solutions are asymmetric, while steady ADI solution is symmetric. Although unsteady LU-SGS solution has fluctuations in the early stage relatively smaller than steady LU-SGS solution, two converged values coincide nearly with the same asymmetric flow. On the other hand, ADI solution is symmetric throughout all the iteration processes. This proves that LU-SGS algorithm, unsymmetric factorization for the crossflow plane, has numerical error enough to induce asymmetry, while ADI symmetric factorization
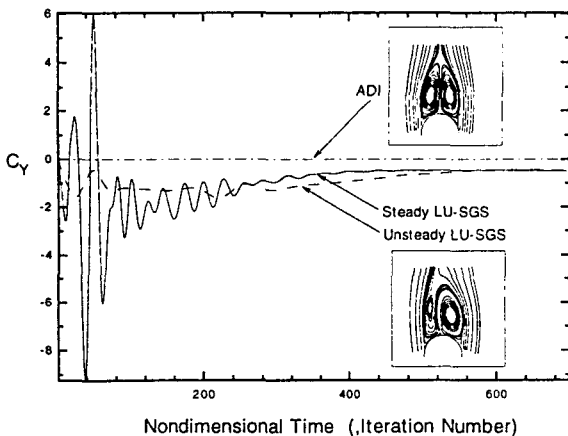
algorithm not, and these results agree with the study of Vanden and Belk.[11] That is, an unsymmetric factorization error for the crossflow plane plays a role of initial asymmetric perturbation, thus can produce asymmetric converged solution.

Note that the computational asymmetric results, like experiments, have not been clearly determined in which direction asymmetric vortex structure occurs. In order to investigate this switching problem, although sweep direction was changed reversely in LU-SGS algorithm, the same result came out. From this fact, it is difficult to conjecture in which direction asymmetric perturbation arisen from numerical factorization error affects. This problem is the pertinent issue which is to be solved in both computations and experiments.

To investigate the effect of initial condition, the above computations were restarted from two symmetric and asymmetric converged solutions respectively. Fig.3 showed that LU-SGS solution with symmetric initial condition is symmetric flow, while ADI solution with asymmetric initial condition is asymmetric condition. These results proved that once converged solution is not affected by factorization method, because unsymmetric factorization error doesn't nearly exist, or even if exists, not enough amount to break symmetry. In the asymmetric case, although small fluctuation is observed, the side-force coefficient finally tends to decrease smoothly toward a constant value.

From above results, we deduce that the unsymmetric factorization error occurs mainly in early computational step and decays to negligible value as it converges. That is, this unsymmetric factorization error in early computational stage is interpreted as a transient disturbance, finally develops entire flowfield into asymmetric flow and continues even when initial asymmetric cause is removed. This concept is absolute instability introduced by Briggs[20] and Bers.[21]
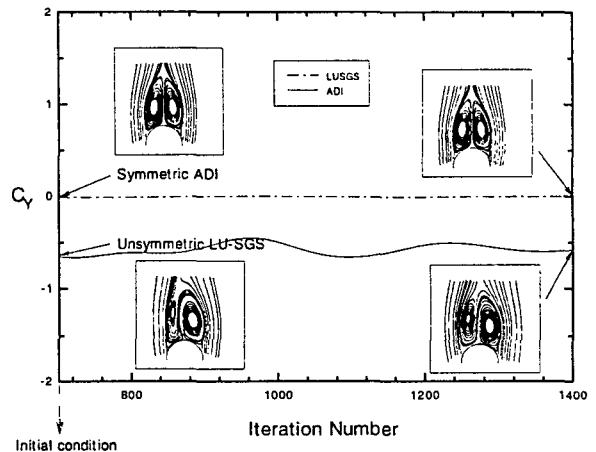
**Fig. 3 Side-force coefficient histories : $M_\infty=0.2$, $\alpha=40$ deg, $Re_D=2.0\times10^5$.**

All the following computations were performed by using LU-SGS unsymmetric factorization algorithm. Therefore naturally perturbed numerical error exists, and may induce asymmetry for perfectly symmetric flow conditions.

*Subsonic, Laminar Flow ($Re_D=2.0\times10^5$, $M_\infty=0.2$)*

The computed circumferential surface pressure distributions for laminar flow ($\alpha=20$ deg) are presented in Fig.4, together with experimental data measured by

**Fig. 2 Side-force coefficient histories : $M_\infty=0.2$, $\alpha=40$ deg, $Re_D=2.0\times10^5$.**

Lamont.[2] At a low angle of attack of 20 deg, the flow, as observed experimentally, is almost symmetric. It can be seen from Fig.4 that the agreement between the computed and measured pressure is very good for all stations.
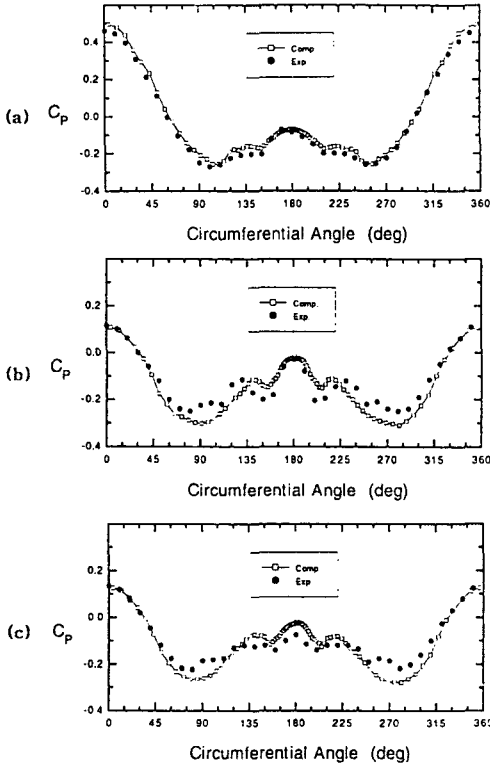


Fig. 4   Computed and measured circumferential surface pressure distributions : $M_\infty=0.2$, $\alpha=20$ deg, $Re_D=2.0\times10^5$ : (a) x/D= 0.5 : (b) x/D = 3.5 : (c) x/D = 5.0.
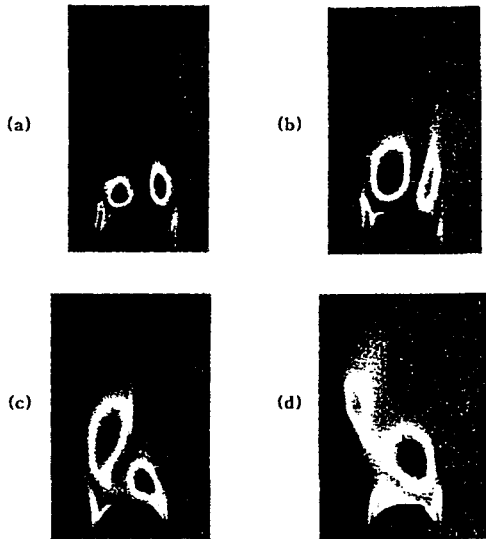


Fig. 5 Total pressure contours at several cross-sections : $M_\infty=0.2$, $\alpha=40$ deg, $Re_D=2.0\times10^5$ : (a) x/D = 3.6 : (b) x/D = 7.1 : (c) x/D = 8.9 : (d) x/D = 11.5.

Computed results for $\alpha=40$ deg, however, large asymmetric vortical flow as observed in many experiments, are shown in Fig.5-8. Computed total pressure and helicity density contours in several cross sections along the body are plotted in Fig.5,6. Helicity density is defined as the scalar product of the local velocity and vorticity vectors. Although both total pressure and helicity density may be good ways of visualizing vortex pattern, total pressure is slightly better between two patterns. But helicity density has advantage of indicating the sense of rotation of vortices.
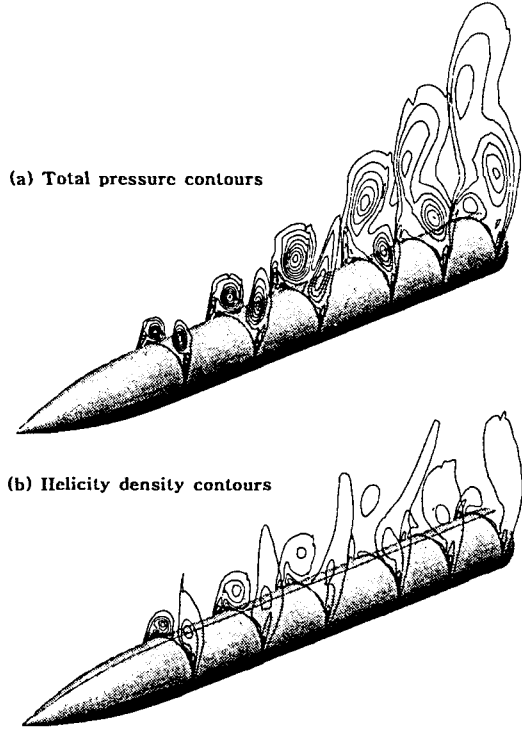


(a) Total pressure contours

(b) Helicity density contours

Fig. 6.  Computational results for $M_\infty=0.2$, $\alpha=40$ deg, $Re_D=2.0\times10^5$.
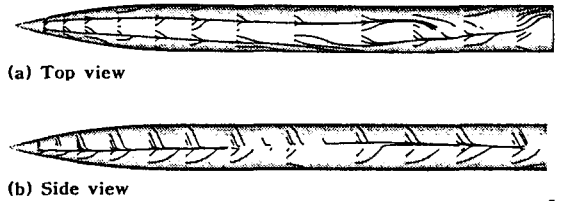


(a) Top view

(b) Side view

Fig. 7 Surface streamlines : $M_\infty=0.2$, $\alpha=40$ deg, $Re_D=2.0\times10^5$.

Fig.7 shows the computed surface flow patterns. Secondary separation line is clearly shown asymmetrically and primary separation line well behaved at $\phi\approx90$ deg. Crossflow streamlines near the leeward surface in several cross sections are also shown in Fig.8. The primary and secondary vortices are clearly observed and asymmetry increases along the downstream. It can be noted that as weakened vortices gradually move upward, they die out at the same time, which should be distinguished from unsteady vortex shedding occurring at much higher angle of attack.
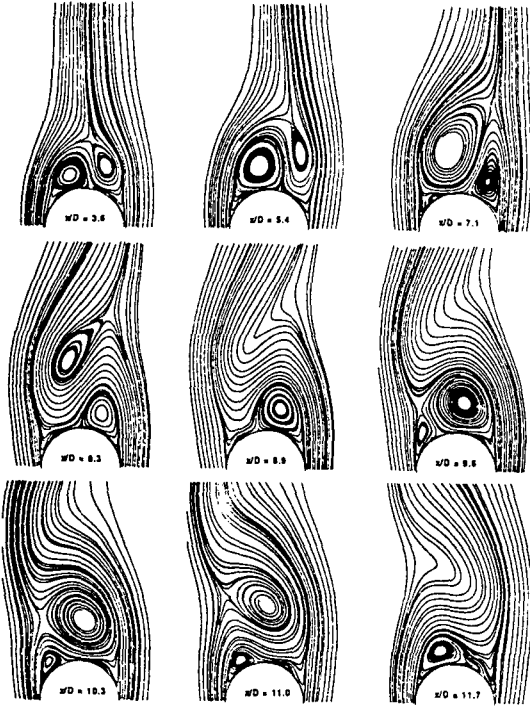
-7-

Fig. 8 Crossflow streamlines near lee-surface on the different cross-sections : $M_\infty=0.2$, $\alpha=40$ deg, $Re_D=2.0\times10^5$.



Fig. 9 Computed and measured circumferential surface pressure distributions : $M_\infty=0.2$, $\alpha=30$ deg, $Re_D=3.0\times10^6$ : (a) x/D= 2.0 : (b) x/D = 3.5 : (c) x/D = 5.0 : (d) x/D = 6.0.

*Subsonic, Turbulent Flow ($Re_D=3.0\times10^6$, $M_\infty=0.2$)*

For the fully turbulent flow, $\alpha=30$ deg, the computed circumferential surface pressure distributions at several axial locations by using Degani-Schiff modified turbulence model are shown in Fig.9, together with Lamont's[3] experimental data. For all axial locations, good agreements are shown, even for the downstream location, although there is slight difference for the location of x/D = 6.0, where significant asymmetry exists. Also noticeable is the
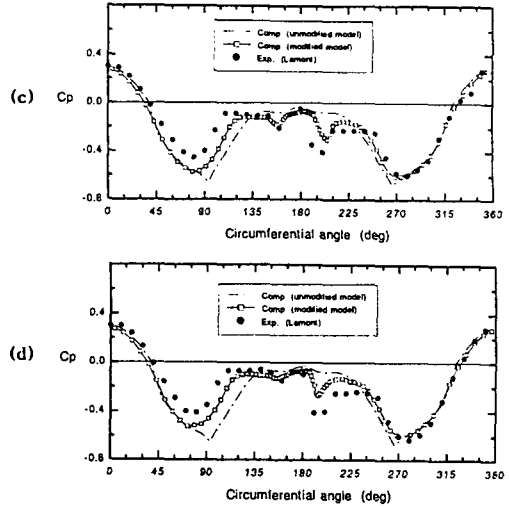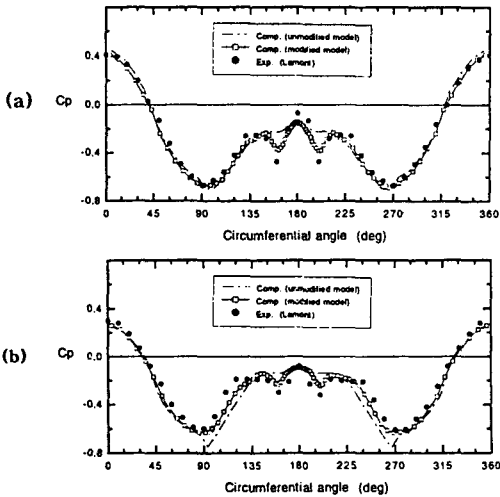


(a) Unmodified turbulence model

(b) Modified turbulence model

Fig. 10 Total pressure contours : $M_\infty=0.2$, $\alpha=40$ deg, $Re_D=3.0\times10^6$.

ability of the numerical solution to reproduce a significant feature of experimental data, namely, the existence and behavior of a sharp local minimum in $C_p$, which is caused by the presence of the secondary vortex at $\phi \approx 180$ deg. On the other hand, the solution for the same flow conditions using the unmodified Baldwin-Lomax turbulence model is far from satisfactory, nearly symmetric flow. The unmodified model in the vortex region yields values of the eddy-viscosity coefficient that are too large as reported by Degani.[7,8] As a result, primary vortex specifically becomes weaker and the amount of asymmetry decreases substantially, as can be seen from the dashed line as indicated in Fig.9.
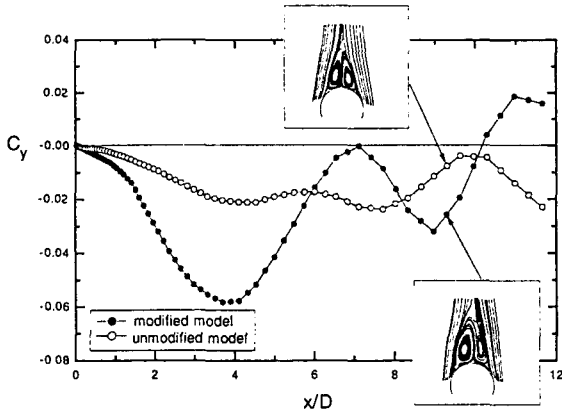


Fig. 11 Sectional side-force distributions : $M_\infty=0.2$, $\alpha=40$ deg, $Re_D=3.0 \times 10^6$.

Total pressure contours are plotted in Fig.10, where using unmodified and modified turbulence model respectively. Fig.10-(a), unmodified model, shows almost symmetric vortices, while the result using the modified model shows asymmetric vortices. The sectional side-force coefficients are shown in Fig.11, where result of the modified model is asymmetric. Otherwise, the case of unmodified model is symmetric, even though is used the same LU-SGS unsymmetric factorization algorithm.

Although the resulting turbulent flow is no longer symmetric, the asymmetry is relatively smaller than that of laminar flow. But Lamont's[2] experiments have reported almost identical side-force between laminar and turbulent flow cases. It can be concluded that although the modified turbulence model phenomenally simulates asymmetric turbulent flow, but is not sufficiently satisfactory for accurate quantitative estimation.

*Supersonic, Laminar Flow ($Re_D=2.0 \times 10^4$, $M_\infty=2.0$)*

It was found that supersonic laminar flow, when using LU-SGS algorithm, converged toward a symmetric solution on a symmetric grid for an angle of $\alpha=30$ deg. It took several times to get solution converged than the subsonic flow computation. This is caused by the fact that the supersonic flow at high angle of attack includes strong shock and expansion waves, and the intense nonlinear waves cause computational difficulties in convergence. The computed sectional side-force coefficients and crossflow streamlines on the leeward surface are shown together with subsonic result in the same Reynolds number, $Re_D=2.0 \times 10^4$, in Fig.12. The figure shows that the supersonic vortices are exactly

symmetric and very large, while subsonic flow is asymmetric and its vortices are relatively small. The result agrees with the experimental results of other investigators,[1] in point that the magnitude of the side-force coefficient generally decreases with increasing Mach number and for Mach numbers greater than 0.8, the side-force coefficient is quite small. Fig.13 shows the crossflow streamlines near the leeward surface in several cross sections for supersonic and subsonic flow for purpose of phenomenal comparison.
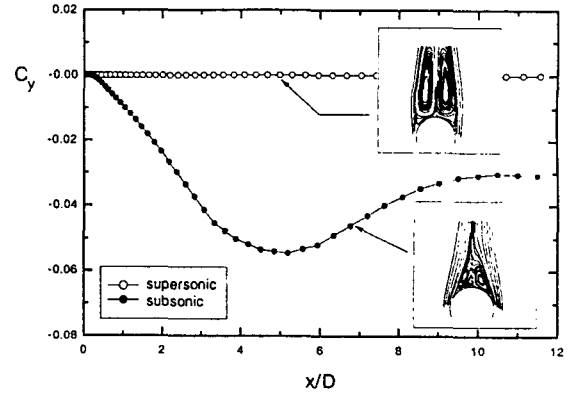


Fig. 12 Sectional side-force distributions : $\alpha=30$ deg, $Re_D=2.0 \times 10^4$ : (supersonic $M_\infty=2.0$, subsonic $M_\infty=0.2$).
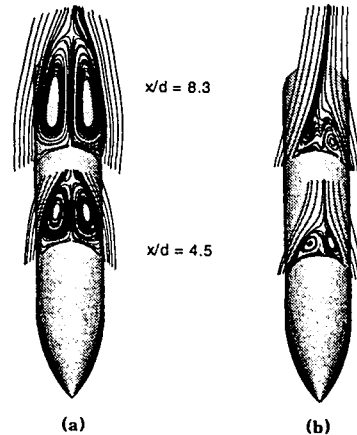


Fig. 13 Crossflow streamlines near lee-surface : $\alpha=30$ deg, $Re_D=2.0 \times 10^4$ : (a) supersonic $M_\infty=2.0$ : (b) subsonic $M_\infty=0.2$.

## CONCLUSIONS

A computational study of the viscous subsonic and supersonic flow over a tangent ogive-cylinder for a range of Reynolds numbers at several high angles of attack suggests the following conclusions.

1) Unsymmetric factorization algorithm, LU-SGS scheme, introduces asymmetric transient error and finally produces asymmetric flow which is classified as absolute instability. When once converged solution is applied to initial condition, no change occurs irrespectively of the algorithms. In conclusion, an unsymmetric factorization error in the early computational stage plays a role of

transient perturbation, finally induces asymmetric vortical flow and continues even when transient factorization error disappears as it converges. These numerical results can be interpreted as absolute-type instability. And computed asymmetric flow is always steady with negligible fluctuations below an angle of attack of 40 deg.

2) For subsonic laminar and turbulent flow, the computed results are in good agreements with measured pressure distributions. The results suggest that the Degani-Schiff modified turbulence model can be utilized to accurately compute the complex asymmetric vortex structure at high angle of attack, while unmodified Baldwin-Lomax model showed symmetric flow inconsistent with experimental results. In turbulent calculations, although the resulting flow is no longer symmetric, the asymmetry is relatively smaller than the existing experimental data. This is recommended that more appropriate turbulence modeling is needed in computation of asymmetric turbulent flow at high angle of attack.

3) The computed supersonic result is symmetric, though unsymmetric factorization algorithm is used, in contrast to asymmetric result of subsonic flow in the same Reynolds number. This result is in agreement with other experimental studies of generally non-existing side-force at that Mach number.

# REFERENCE

[1]Deffenbaugh, F. D., and Koerner, W. G., "Asymmetric Vortex Wake Development on Missiles on High Angle of Attack," *Journal of Spacecraft*, Vol. 14, No. 3, 1977, pp. 155-162.

[2]Lamont, P. L., "Pressure Around an Inclined Ogive Cylinder with Laminar, Transitional, or Turbulent Separation," *AIAA Journal*, Vol. 20, No. 11, 1982, pp. 1492-1499.

[3]Lamont, P. J., "The Complex Asymmetric Flow Over a 3.5D Ogive Nose and Cylindrical Afterbody at High Angles of Attack," AIAA Paper 82-0053, Jan. 1982.

[4]Zilliac, G. G., Degani, D., and Tobak, M., "Asymmetric Vortices on a Slender Body of Revolution," *AIAA Journal*, Vol. 29, No. 5, 1991, pp. 667-675.

[5]Degani, D., "Effect of Geometrical Disturbance on Vortex Asymmetry," *AIAA Journal*, Vol. 29, No. 4, 1991, pp. 560-566.

[6]Degani, D., and Schiff, L. B., "Numerical Simulation of the Effect of Spatial Disturbances on Vortex Asymmetry," *AIAA Journal*, Vol. 29, No. 3, 1991, pp. 344-352.

[7]Degani, D., Schiff, L. B., and Levy, Y., "Numerical Prediction of Subsonic Turbulent Flows over Slender Bodies at high Incidence," *AIAA Journal*, Vol. 29, No. 12, 1991, pp. 2054-2061.

[8]Degani, D., and Levy, Y., "Asymmetric Turbulent Vortical Flows over Slender Bodies," *AIAA Journal*, Vol. 30, No. 9, 1992, pp. 2267-2273.

[9]Siclari, M. J., and Marconi, F., "The Computation of Navier-Stokes Solutions Existing Asymmetric Vortices," AIAA Paper 89-1817, June 1989.

[10]Hartwich, P. M., Hall, R. M., and Hemsch, M. J., "Navier-Stokes Computations of Vortex Asymmetries Controlled by Small Surface Imperfections," AIAA Paper 90-0385, Jan. 1990.

[11]Vanden, K. J., and Belk, D. M., "Numerical Investigation of Subsonic and Supersonic Asymmetric Vortical Flow," AIAA Paper 91-2869-CP, 1991.

[12]Thomas, J. L., "Reynolds Number Effects on Supersonic Asymmetrical Flows over a Cone," *Journal of Aircraft*, Vol. 30, No. 4, 1993, pp. 488-495.

[13]Yang, X., and Zebib, A., "Absolute and convective Instability of a Cylinder Wake," *Physics of Fluids*, Vol. 1, No. 4, 1989, pp. 689-696.

[14]Beam, R. M., and Warming, R. F., " An Implicit Factored Scheme for the Compressible Navier-Stokes Equations," *AIAA Journal*, Vol. 16, No. 4, 1978, pp. 393-402.

[15]Yoon, S., and Jameson, A., "Lower-Upper Symmetric-Gauss-Seidel Method for the Euler and Navier-Stokes Equations," *AIAA Journal*, Vol. 26, No. 9, 1988, pp. 1025-1026.

[16]Yoon, S., and Kwak, D., "Implicit Navier-Stokes Solver for Three-Dimensional Compressible Flows," AIAA paper 91-1555-CP, 1991.

[17]Baldwin, B., and Lomax, H., "Thin-Layer Approximation and Algebraic Model for Separated Turbulent Flows," AIAA Paper, 78-0257, Jan. 1978.

[18]Degani, D., and Schiff, L. B., "Computation of Turbulence Supersonic Flows Around Pointed Bodies Having Crossflow Separation," *Journal of Computational Physics*, Vol. 66, No. 1, 1986, pp. 173-196.

[19]Gee, K., Cummings, R. M., and Schiff, L. B., "Turbulence Model Effects on Separated Flow About a Prolate Spheroid," *AIAA Journal*, Vol. 30, No. 3, 1992, pp. 655-664.

[20]Briggs, R. J., "Electron-Stream Interaction with Plasmas," Research Monograph 29, MIT Press, Cambridge, MA, 1964.

[21]Bers, A., "Handbook of Plasma Physics," North-Holland, New-York, 1983, pp. 452-516.